AEROSPACE REPORT NO.
TOR-2018-02829

An AE9/AP9 Kernel for Ionizing Dose from Electrons Incident on Hollow Aluminum Shells

October 15, 2019

T. P. O'Brien and M. D. Looper
Space Sciences Department
Space Science Applications Laboratory

Prepared for

Space and Missile Systems Center
Air Force Space Command
483 N. Aviation Blvd.
El Segundo, CA 90245-2808

Contract No. FA8802-19-C-0001

Authorized by: Space Systems Group

Acknowledgments

The authors acknowledge useful discussions with H. O'Donnell regarding the merit of spherical shell relative to solid sphere.

Abstract

The AE9/AP9 project has developed several "kernels" that relate particle flux to radiation effects through pre-computed linear transforms. For ionizing dose, the widely used tool SHIELDOSE-2 has been adapted to kernels for solid spherical shielding, slab shielding, and semi-infinite shielding. This report describes a new idealized geometry: hollow spherical shell. In some ways, a hollow spherical shell is more representative of the box geometry found in spacecraft than the solid-sphere geometry provided by SHIELDOSE-2. The hollow spherical shell kernel is constructed by simulating electrons incident on hollow aluminum shells of various thicknesses with a silicon target at their center. For protons, it is argued that there is no need for a distinct kernel for hollow shell rather than solid sphere. For electrons only, the response function of dose in the silicon inside the hollow aluminum spheres is tabulated in the kernel, and metadata describing the kernel units, as well as energy and shielding depth grids, are included in an eXtensible Markup Language (XML) text file conforming to the AE9/AP9 kernel format standard. The kernel is compared to industry standard tools and found to be in good agreement. During our development of the hollow-shell kernel, we determined that further work will be needed to establish best practices for adequately capturing dose due to tertiary or reconversion electrons produced by bremsstrahlung in thick shields.

Contents

Figure

1. Introduction

An AE9/AP9 kernel transforms particle flux or fluence *j(E)* as a function of energy *E* into some desired radiation effect such as dose *d(T)* versus depth *T* [5][6]. Kernels only apply for effects that are linear functions of the incident flux. The kernel approximates the convolution integral:

$$d(T) = \int G(E;T)j(E)dE \tag{1}$$

In practice, this integral is represented by the kernel as a matrix-vector transform:

$$\vec{d} = \underline{\underline{A}}\vec{j} \tag{2}$$

where

$$d_i = d(T_i) \tag{3}$$

$$A_{ik} = G(E_k;T_i)\Delta E_k \tag{4}$$

$$j_k = j(E_k) \tag{5}$$

Developing a kernel usually amounts to determining the transform matrix $\underline{\underline{A}}$ from a physics calculation. In this report, we describe development of a kernel matrix for electrons incident on hollow spherical shells reaching a silicon target centered inside.

Once the kernel is computed, the matrix A_{ik}, the incident energies E_k, and the output depths d_i along with units and other metadata are stored in an eXtensible Markup Language (XML) text file that is both human and machine readable and that conforms to a published format specification for AE9/AP9 kernels [6]. The AE9/AP9 application can read kernel XML files at runtime to incorporate the spherical shell kernels and other radiation effects kernels into the runtime statistical analysis machinery of the application. We will argue that because proton scattering in shielding is minimal, the hollow-shell and solid-sphere kernels for protons would be essentially identical, so no separate proton shell kernel is needed.

2. Hollow Spherical Shell Geometry and Geant4 Runs

While conceptually simple, the calculation of the spherical shell response using numerical simulation tools proved more complex than initially expected. In this section, we lay out the geometry of the simulation, the forward and adjoint methods used, a study of the effect of target radius and shell inner radius, and a discussion of separating electron and photon contributions to dose.

2.1 Geometry

The long-standard SHIELDOSE and SHIELDOSE-2 dose-depth codes [7] allow calculation of the ionizing radiation dose caused by isotropic monoenergetic protons or electrons in a silicon target under an aluminum shield of varying thickness and configuration. The result of this calculation can be convolved with a particle energy spectrum in a manner analogous to our kernel technique, and we have in the past translated SHIELDOSE-2 results into the kernel format that allows them to be used with AE9/AP9. One of the shielding geometries available in SHIELDOSE-2 places an infinitesimal silicon target at the center of a solid sphere of aluminum that has a radius that constitutes the thickness of the given shield. This geometry, illustrated in Figure 1(a), is used to give a worst-case estimate of dose or dose rate because (1) it is illuminated by incident energetic particles from all sides (whereas the other SHIELDOSE-2 geometries are planar and illuminated from only one side) and (2) the thickness of shielding is the same in all directions outward from the silicon target (whereas for planar geometries, obliquely incident particles will have a nominal (straight) path through the shielding increased by the secant of the incidence angle).

We have developed an AE9/AP9 kernel to perform the same calculation of radiation dose for a new geometry, a hollow spherical aluminum shell, as illustrated in Figure 1(b). This geometry retains the illumination from all sides that is characteristic of the SHIELDOSE-2 solid-sphere geometry, but adds an element of realism in that dose-sensitive electronic parts of concern are usually not pressed right up against the bulk of the shielding, as is implicitly the case in the solid-sphere geometry. In addition to the shielding thickness, labeled T in Figures 1(a) and 1(b), this new geometry adds a second parameter, the inside radius of the sphere, labeled R in Figure 1(b). We have explored the effect of varying this parameter on the result of dose calculations, in addition to comparing those results between hollow and solid spherical geometries, and we have found that the inside radius of the hollow shell has a negligible influence on the result so that our results are representative of dose to, for example, sensitive parts inside electronics boxes of a variety of sizes. This will be discussed in detail in the following sections.

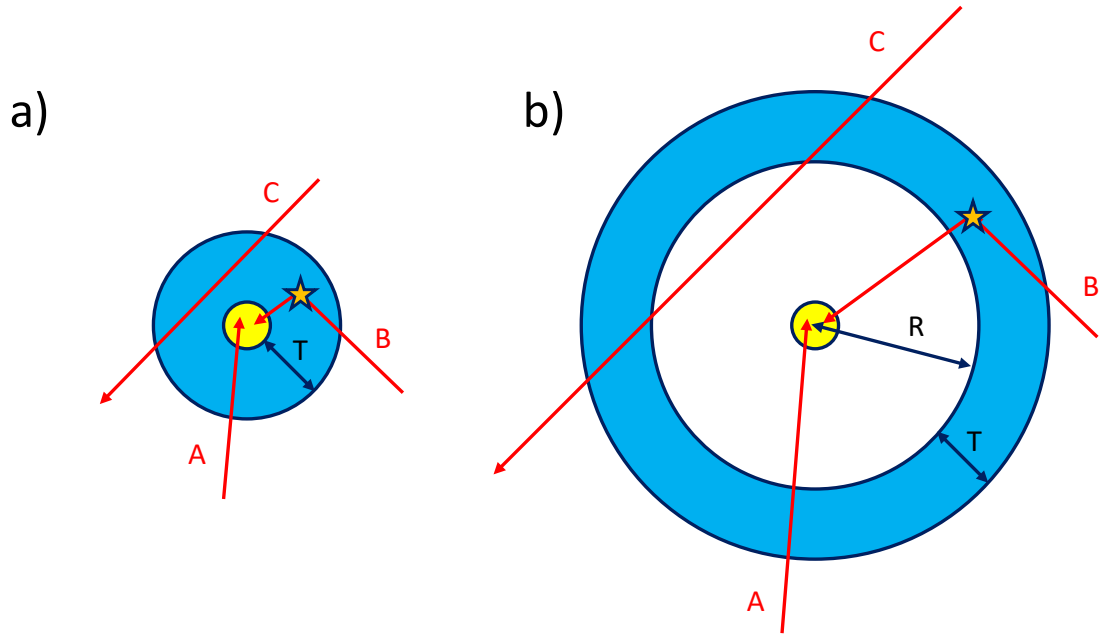

Figure 1. Shielding geometries and trajectories. (a) represents the solid-sphere geometry as modeled by SHIELDOSE-2, and (b) depicts the hollow spherical shell addressed by our new hollow-shell kernel. Yellow represents the spherical silicon target in which dose is measured under the blue aluminum shield. *T* is the thickness of the shield in both cases, and *R* is the inside radius of the shell for (b). Trajectories labeled A, B, and C are discussed in the main text.

2.2 Forward Monte Carlo Simulations

The Geant4 open-source radiation transport code [1] models the transport of energetic particles through a user-defined geometry, tabulating any quantities of interest, such as energy deposit, in a sensitive target within the geometry. The standard use of the code is for forward Monte Carlo simulations, in which individual particles are transported forward in time subject to all relevant physical processes, such as energy loss, scattering, and production of secondary particles, with stochastic processes being modeled by sampling from the probability distributions of the outcomes of those processes. This gives a very accurate representation of quantities, such as ionizing energy deposit (radiation dose) in a target, because with enough simulated primary particles, the calculation will include the effects of rare events like, for example, the trajectories labeled B in Figures 1(a) and 1(b), where the primary particle would not have intersected the target along its initial trajectory but scattering or the production of a secondary particle caused a particle to do so (e.g., [3]). However, because it must also model trajectories like those labeled C that never affect the target, it can get computationally very expensive to build up statistics for quantities affecting a small sensitive target inside a large geometry.

We were interested in developing a kernel to represent radiation dose under shielding thicknesses from 10 mils to 10 inches of aluminum, and we started by running Geant4 forward Monte Carlo simulations for protons and electrons at a set of discrete energies, isotropically incident on such shielding geometries. However, because the target needs to have uniform dose throughout it in order to represent a tiny electronic part, we found that a target even as large as a sphere 1 mm in radius was too thick so that dose in its outer layers was greater than that at its core; and for such a small sensitive target in such a large simulation volume, we found that we were unable to achieve reasonable result statistics, even after long runtimes, for shield thicknesses greater than about 1 inch. However, Geant4 has also enabled us to perform alternative radiation-transport calculations with much greater speed at some sacrifice in physical accuracy, as detailed by [4], and we turned to these alternative techniques to complete the task.

2.3 Protons—Straight-Line Trajectories

Because protons scatter much less than electrons at the energies of interest for AE9 and AP9, trajectories like those labeled B in Figures 1(a) and 1(b) are comparatively rare and their contributions to dose are much less than those of straight-in trajectories like those labeled A in those figures. Thus, we can, as an approximation, only consider the energy deposited by protons like those labeled A, which travel along trajectories already aimed at the target from the outset. In this case, though, the pathlength through shielding of all trajectories that can contribute to radiation dose is nearly the same for a target that is small compared to the thickness of the shield. Any trajectory like those labeled A in Figures 1(a) and 1(b) must come in nearly perpendicular to the outside of the shield in order to reach the target at the center, regardless of the inside radius of the shield (equal to target radius for the solid-sphere geometry). The difference in pathlength through the shield among all such trajectories will be, at most, of the same order as the size of the target.

Reference [4] examined the further approximation of considering proton range and energy to be deterministic with no fluctuations, called the Continuous Slowing-Down Approximation (CSDA). However, for our purposes here, we only need to note the similarity of pathlengths remarked on above, which implies that for a given shield thickness, the dose in our spherical shell geometry should be very close to that in the SHIELDOSE-2 solid-sphere geometry. This means that one might as well use the full SHIELDOSE-2 calculation, which includes results of Monte Carlo simulations of dose rather than using the CSDA; in particular, this will be more accurate for high-energy protons, since the CSDA does not include the extra dose from nuclear fragments produced in the shield [4]. Thus, we will not further pursue the development of a separate hollow-shell dose calculation for protons.

2.4 Electrons—Adjoint Monte Carlo Simulations

For electrons, a faster alternative to a forward Monte Carlo simulation is an adjoint Monte Carlo simulation. In this technique, particles are launched outward from the sensitive target and are propagated backward in time with potential stochastic processes like scattering, energy loss fluctuations, or generation by a different primary particle (possibly of a different species, for example, with a photon modeled as having been generated by bremsstrahlung from a primary electron) being sampled from probability distribution functions. Reference [4] compared forward and adjoint simulations of energy deposit in a simple geometry and found that the adjoint technique as implemented in Geant4 gave good results for electrons but not for protons. Adjoint simulations build up statistics much faster than forward simulations for a small target in a large geometry, because only trajectories like those labeled A and B in Figures 1(a) and 1(b) are considered and no time is wasted calculating trajectories like those labeled C.

Figures 2 and 3 compare the results of Geant4 forward and adjoint simulations for the solid-sphere geometry with shielding thicknesses ranging from 10 mils to 1 inch. Because the adjoint technique begins with particles at the target, it implicitly ranges over a continuous external primary spectrum that could have produced those particles at the target, so these results are plotted as lines. The forward technique starts with arbitrary external particles, so we simulated the discrete energies that are presented as dots. The quantity plotted as the ordinate is the dose response in the target to primary electrons at the energy plotted as the abscissa; this quantity is to be convolved with a differential, directional fluence in units of electrons per (cm^2 sr MeV) to give a dose, or with a flux in units of electrons per (cm^2 sr MeV sec) to give a dose rate. (Reference [4] discusses this, along with the calculations needed to scale the results of either a forward or adjoint Monte Carlo simulation into such a dose response.)

Various spikes larger than the apparent magnitude of statistical fluctuations are apparent in the adjoint results. These are the result of a rare but documented error in the Geant4 implementation of this technique, which results in an anomalously high weight being assigned to certain trajectories that make an

anomalously high contribution to dose in this calculation. These spikes have been left in Figures 2 and 3 to show the magnitude of the issue; however, they are corrected for in subsequent figures and in the calculations that we used to build the kernel. To do this correction, we performed the full set of simulations (initial forward or adjoint particle, energy, shielding geometry and thickness) for 10 independent seeds of the Geant4 random-number generator. For each primary electron energy (discrete initial value for forward simulations or point composing the curves for adjoint), we computed the standard deviation among these 10 results, and if one of the 10 results was more than 2.9 times this standard deviation away from the mean, we discarded it and recalculated the mean. In the limiting case where one of the 10 samples is so much larger than the others that their values are negligible by comparison, the mean will be 1/10 of the value of the large sample and the standard deviation will be 3 times the mean, so the anomalous value will be 3 times the standard deviation away from the mean.

Looking at Figure 2, we see very good agreement, within about 10%, between the forward dots and adjoint curves, apart from the spikes in the latter. Figure 2 has a target with 1 mm radius at the center of the aluminum sphere; Figure 3 is for a target 10 times smaller, to improve uniformity of dose. This means that only a tenth as many primary electrons are expected to travel through the shield to deposit energy in the forward simulations as for the 1 mm case. The error bars (standard deviation of the mean) bear this out, and again, we did not even try to simulate shields thicker than 1 inch. (Error bars were smaller than the dots in most cases in Figure 2, so we did not plot them even when they would not have been that small to the lower left.) Thus, the advantage of the adjoint method is clear in this regard. Next, we will consider the effects of the different target sizes and the other geometric parameters.

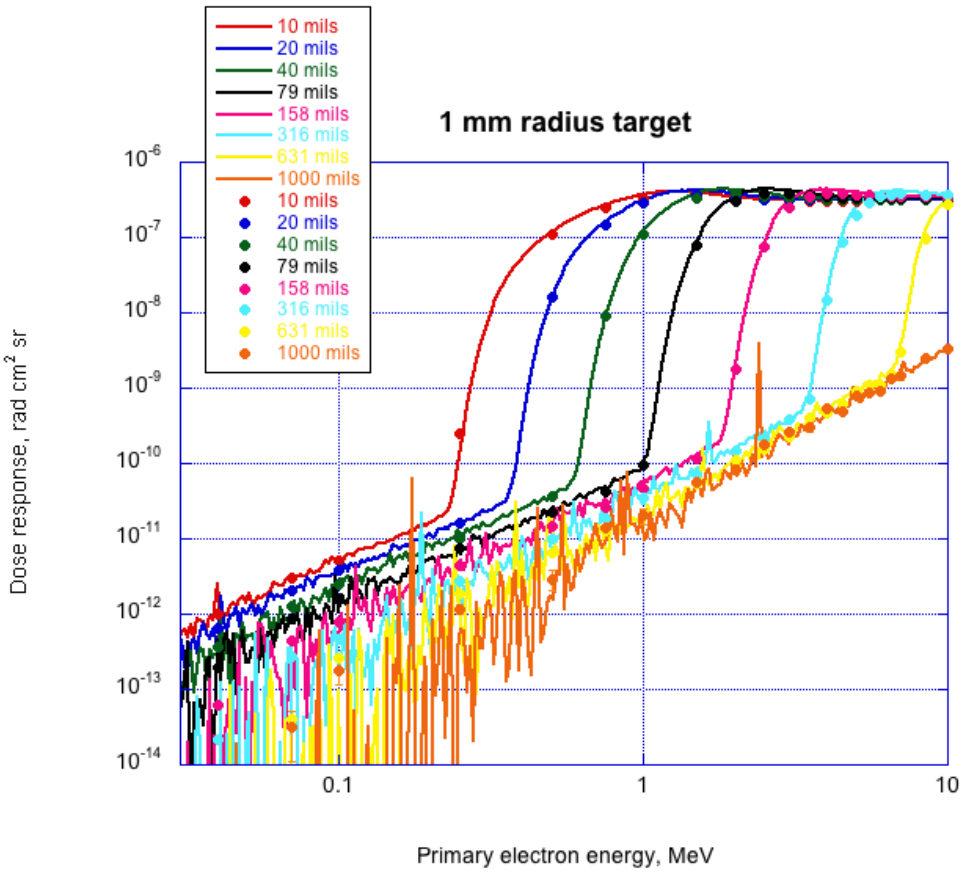

Figure 2. Comparison of forward (dots) and adjoint (lines) Monte Carlo simulation results for dose response as a function of primary electron energy in a 1 mm radius target under solid-sphere shielding from 10 mils to 1 inch thick.

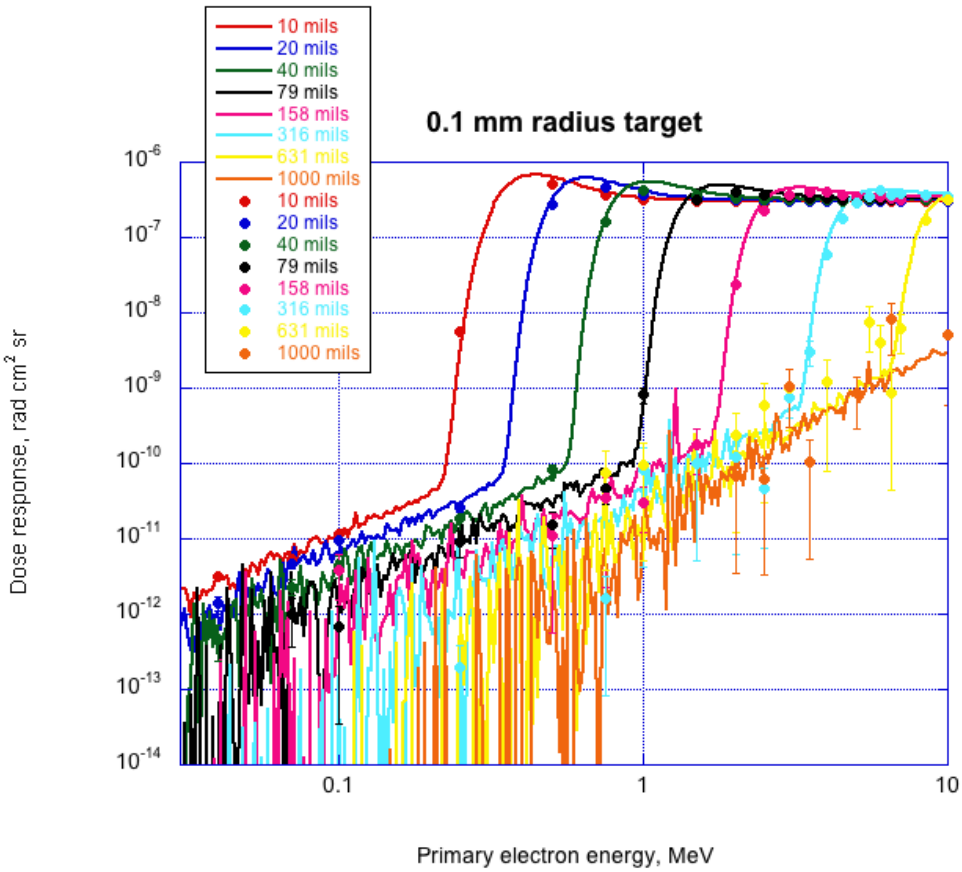

Figure 3. Comparison of forward (dots) and adjoint (lines) Monte Carlo simulation results for dose response as a function of primary electron energy in a 0.1 mm radius target under solid-sphere shielding from 10 mils to 1 inch thick.

2.5 Effects of Target Size and Shell Inner Radius

The differences between the adjoint curves in Figure 2 and the corresponding curves in Figure 3 clearly show that a 1 mm radius target is too large for this calculation. For primary electron energies near the threshold where the curves rise sharply, a substantial amount of the energy reaching the target through the shield is carried by electrons and photons with ranges shorter than the radius; therefore, they deposit their energy in the outer layers of the target. However, the dose is calculated as energy deposit divided by target mass, so the reported dose is artificially low because the unaffected mass deeper inside the target is counted in the denominator.

Figure 4 replicates the adjoint curves in Figure 3, with the de-spiking correction applied as discussed above, and adds more adjoint results for thicknesses up to 10 inches in the solid-sphere geometry. The actual set of thicknesses simulated was 3 times as dense (with 31 values logarithmically spaced between 10 mils and 10 inches) but only a subset is shown here for clarity. Figure 5 is for a target 10 times smaller than the one in Figures 3 and 4 and shows a slight further shift in the curves near threshold, indicating that even the 0.1 mm radius in those figures was still slightly too large for dose uniformity. Another factor of 10 smaller makes even less difference (shown later).

Turning now to the question of the effect of a nonzero inner radius on a hollow spherical shell shield, Figure 6 stays with the 0.01 mm radius target of Figure 5, but moves the shield out from the target to a

1 cm inner radius. The curves flatten out, almost as if the target were too thick again; however, in this case it is due to the fact that secondary particles from an electromagnetic shower near the inner edge of the shell can fly by and miss the detector without depositing energy, whereas there is no room to miss in the solid-sphere geometry. The difference between dose responses under spherical shell and solid-sphere shields is largest at primary electron energies just above the threshold for penetration of a given shield thickness because the shower is broadest where the energies of the penetrating electron and its accompanying shower particles are lowest; therefore, they scatter more before exiting the shield. At higher primary electron energies, the difference is reduced because the higher-energy penetrating electron is accompanied by a narrower shower of secondaries.

Figures 7 and 8 show the results for the 0.01 mm radius target as the spherical shell's inner radius moves out to 10 and 100 cm, and, perhaps surprisingly, there is little difference between these and Figure 6 and almost no difference between Figures 7 and 8. The spreading of the multiple secondary particles in an electromagnetic shower, as discussed above, can only go so far before only one of the particles at a time will hit the target (all of them will hit it in the solid-sphere geometry), and after that, the increasing inner surface area of the shell provides an additional source that balances the spreading, $1/R^2$ versus $1/R^2$. Thus, for an inner radius larger than about 1 cm, the results are independent of that inner radius, and we can speak simply of a hollow spherical shell shielding geometry without having to specify a radius.

To check that 0.01 mm was a small enough radius for the silicon target, we ran the sets of cases (energy, thickness) for the solid sphere and 10 cm inner radius geometries but with the target another factor of ten smaller (0.001 mm). The results are shown in Figures 9 and 10, to be compared with Figures 7 and 5, respectively. These figures reveal that target size may actually become *too* small, a subject we will next study in detail.

Every electron at the target will deposit energy uniformly along its path. However, the probability that photons in the target will interact with it and deposit energy declines with thinner targets. Thus, having the target too large (so that we get self-shielding) will result in too little dose response being calculated above the threshold of electron penetration in particular, but having it too large (so that we miss photons) will result in too little dose response being calculated *below* that threshold where bremsstrahlung photons are the dominant particles reaching the target. Initially we attempted to resolve this issue by simulating several target sizes and taking the maximum dose response from any target size. However, we ultimately settled on a subtler approach: using electron energy deposits calculated for a smaller target and photon energy deposits calculated for a larger target.

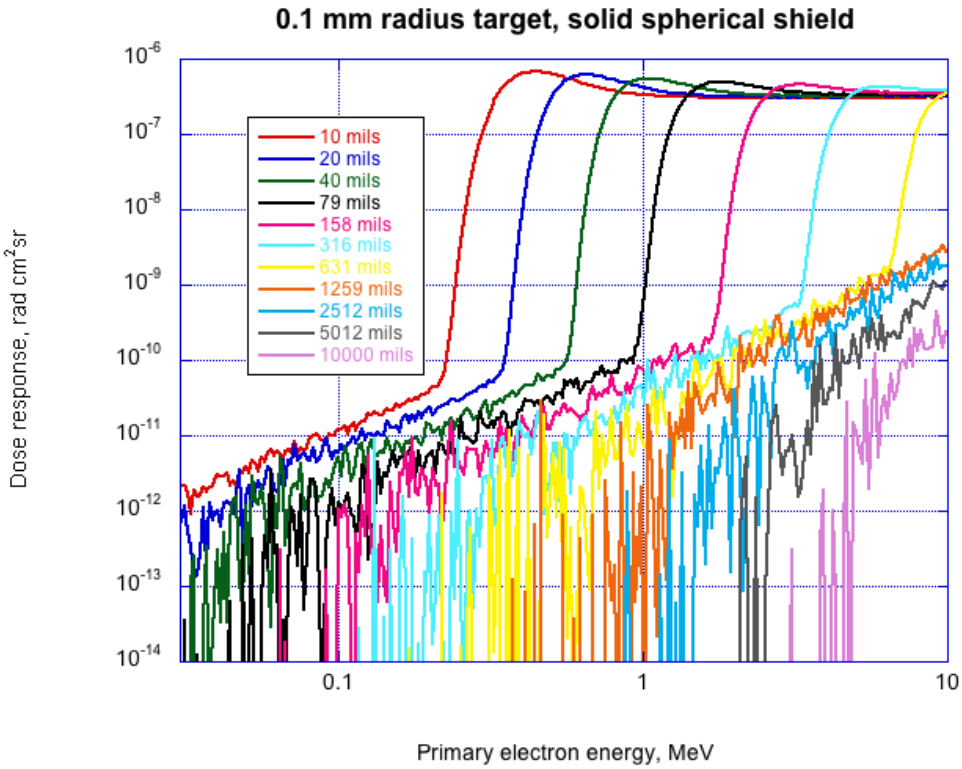

Figure 4. Adjoint Monte Carlo simulation results for dose response as a function of primary electron energy in a 0.1 mm radius target under solid-sphere shielding from 10 mils to 10 inches thick with spikes removed, as described in the main text.

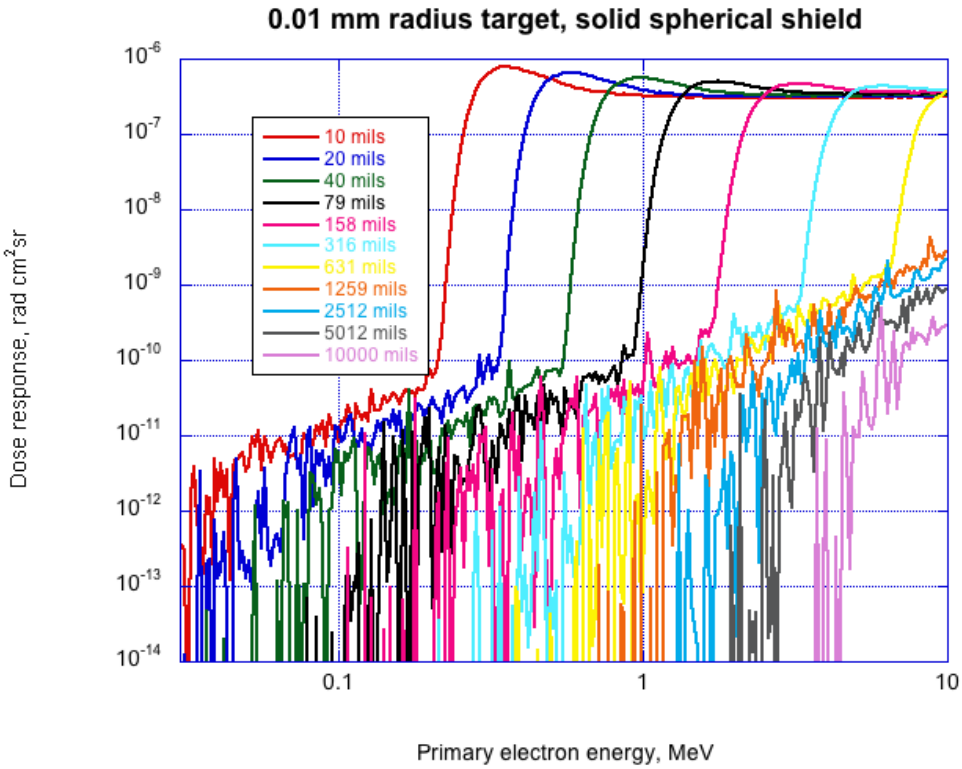

Figure 5. Adjoint Monte Carlo simulation results for dose response as a function of primary electron energy in a 0.01 mm radius target under solid-sphere shielding.

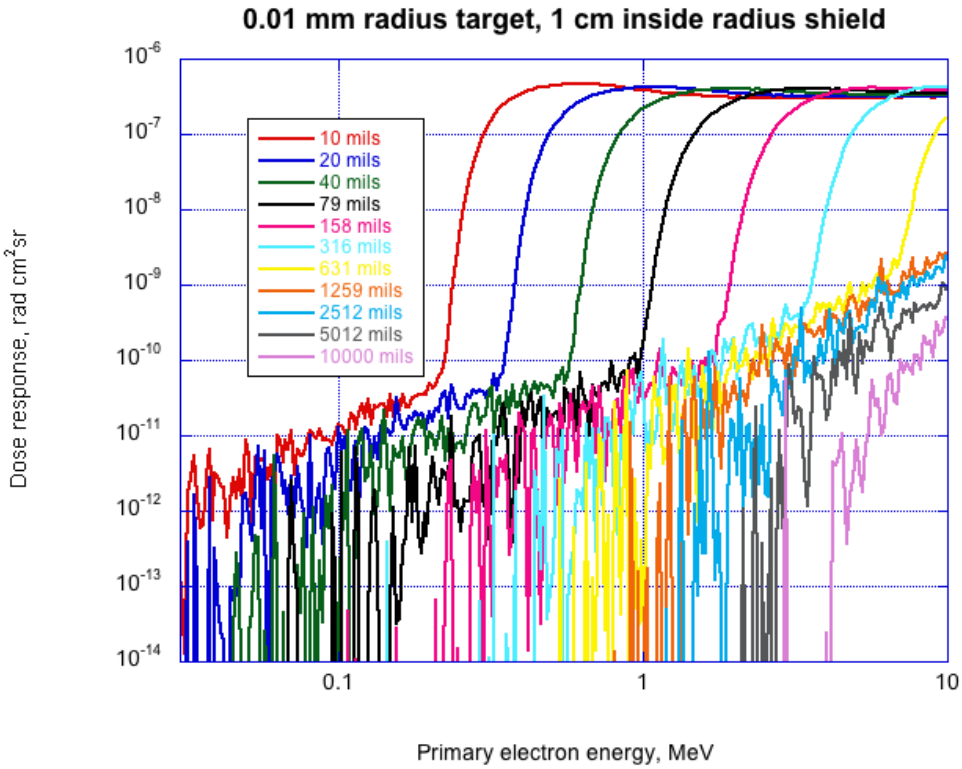

Figure 6. Adjoint Monte Carlo simulation results for dose response as a function of primary electron energy in a 0.01 mm radius target under hollow spherical shell shielding with 1 cm inside radius.

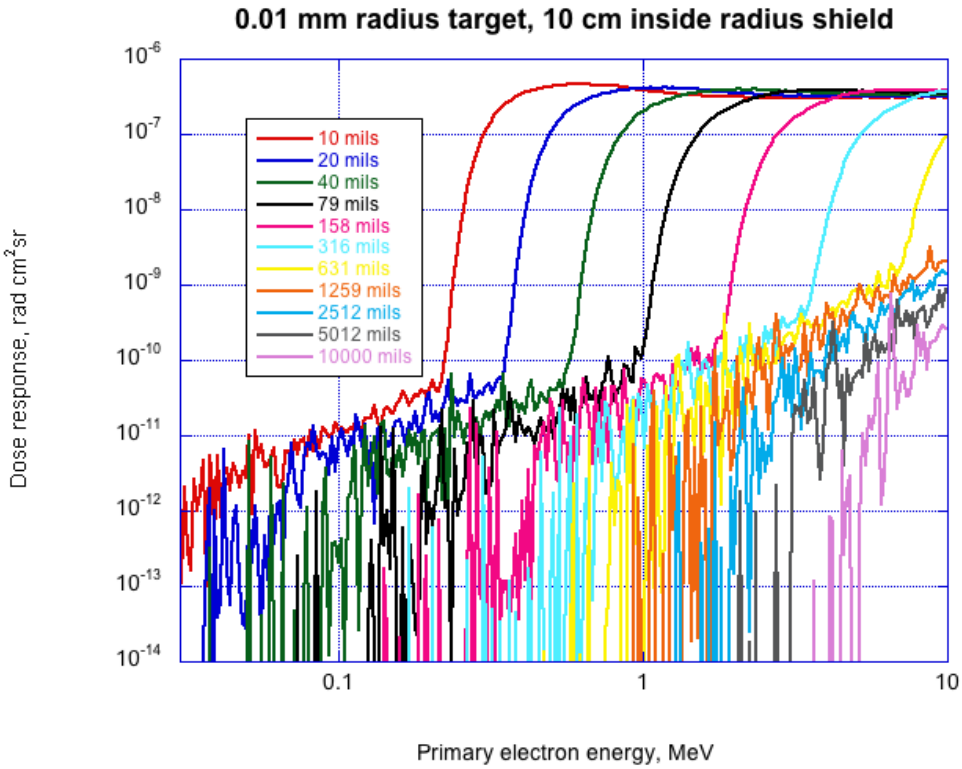

Figure 7. Adjoint Monte Carlo simulation results for dose response as a function of primary electron energy in a 0.01 mm radius target under hollow spherical shell shielding with 10 cm inside radius.

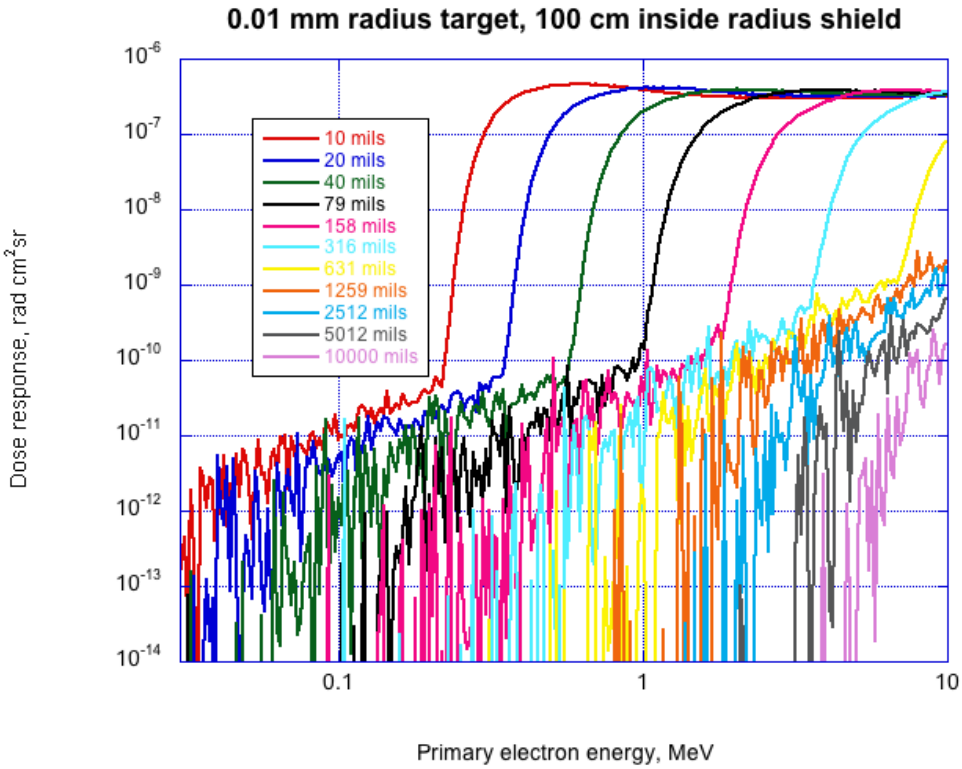

Figure 8. Adjoint Monte Carlo simulation results for dose response as a function of primary electron energy in a 0.01 mm radius target under hollow spherical shell shielding with 100 cm inside radius.

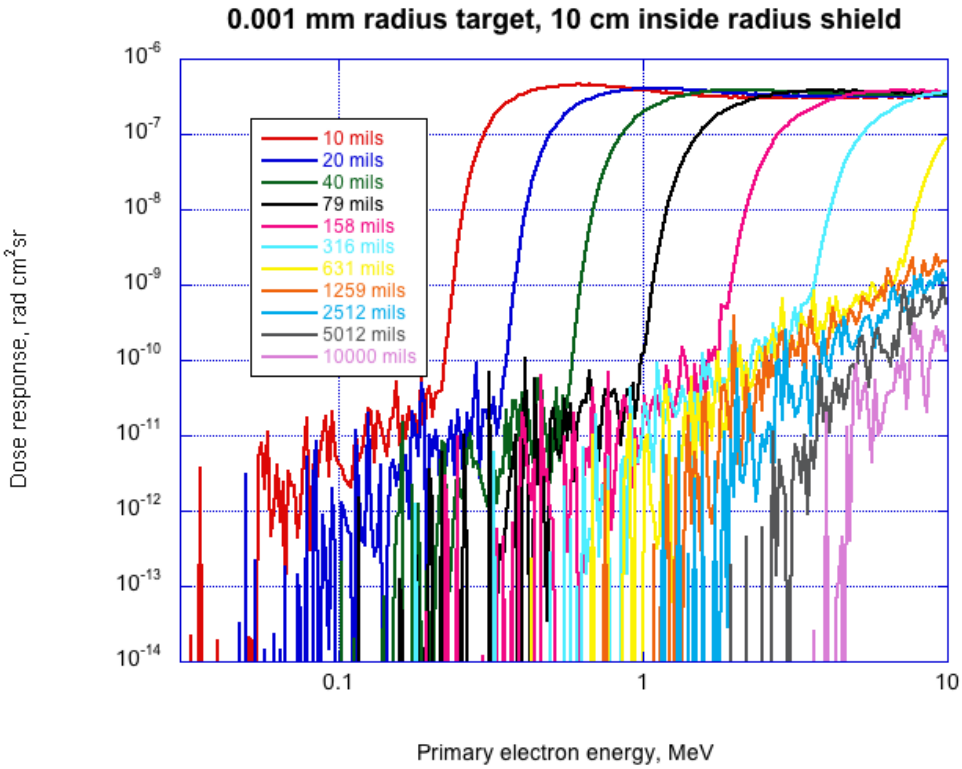

Figure 9. Adjoint Monte Carlo simulation results for dose response as a function of primary electron energy in a 0.001 mm radius target under hollow spherical shell shielding with 10 cm inside radius.

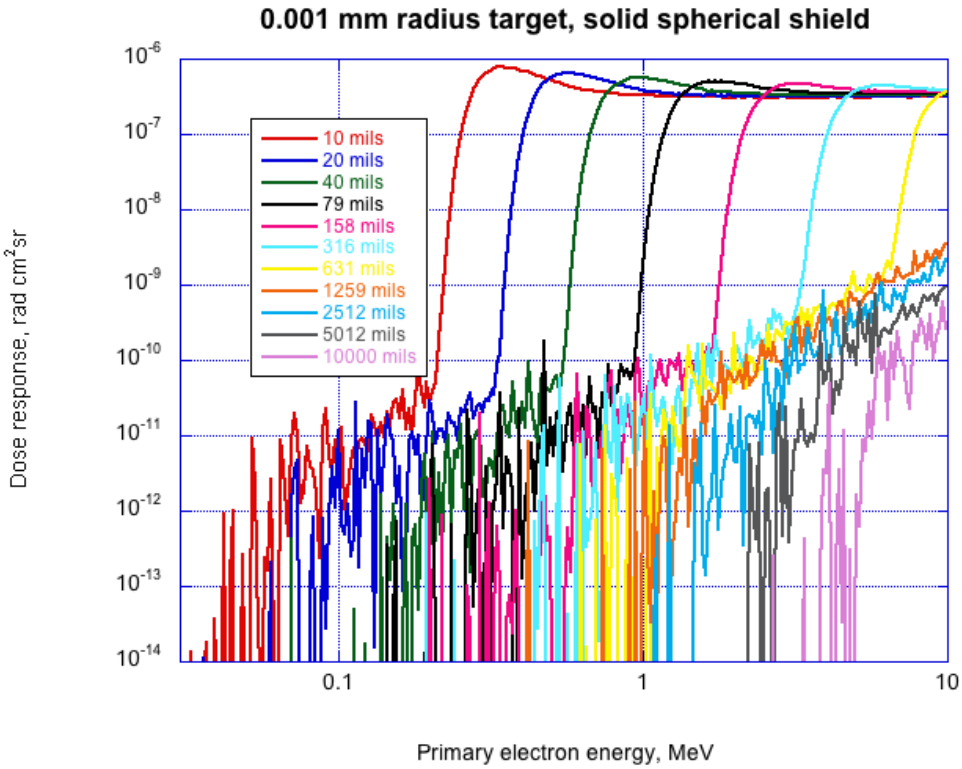

Figure 10. Adjoint Monte Carlo simulation results for dose response as a function of primary electron energy in a 0.001 mm radius target under solid-sphere shielding.

2.6 The Hybrid Target Solution

For construction of the final kernel, we determined that a silicon target of diameter 300 nm captured the dose response due to photons at the target, while a target of diameter 10 nm captured the electron response. First, we performed forward Monte Carlo simulations of the dose response of photons and electrons over a range of energies on bare silicon spheres of varying diameters. This allowed us to determine at what thickness self-shielding is an issue, and at what thickness the target is too small to absorb photon energy. Figure 11 shows this calculation for photons and Figure 12 shows this calculation for electrons. Together, these calculations inform us that a good choice for the photon target is 300 nm, and a good choice for the electron target is 10 nm. For the electrons, the choice is obvious as the 10 nm target eliminates self-shielding and undesired effects related to capture of secondary particles, as labeled in the figure. ("Overshoot" is analogous to the difference discussed in section 2.5 between dose at threshold for a solid spherical shield versus a hollow shell, where showers of secondary particles spread out around the initial electron's trajectory and are absorbed too effectively in the outer layers of the target, while "secondary recapture" occurs when the target is thick enough for secondary particles to experience self-shielding even if the primary electrons do not.) For the photons, the choice is made to favor larger response to low-energy photons, which are expected to be more common under shielding for realistic electron spectra incident on the outside of space vehicles, while avoiding self-shielding.

In order to compute the full dose response due to both photons and electrons for these two targets, separately, we performed adjoint simulations to determine the spectra of both electrons and photons at the

target for each given energy of primary electrons incident on each spherical Al shell. By symmetry, the angular distribution of these particles is isotropic at the surface of a target that is small compared to the outside radius of the shield. By convolving these electron and photon spectra at the target from adjoint simulations with the respective forward simulations of the dose response of the bare detector, we can determine the dose response for each incident electron energy for either silicon target, broken out by photons on a 300 nm target and electrons on a 10 nm target. This combination of forward (into the target) and adjoint (through the shield) calculations greatly improves the statistics of dose response for photons in particular, because, as seen in Figure 11, we can obtain good statistics for any photon's average energy deposit into the target. By contrast, the Geant4 implementation of the full adjoint technique (through the shield and into the target) simulates a single interaction with the target for each photon, and so many simulated events contribute nothing to the average as the photon simply passes through the target.

We note that in the case of electrons reaching the target, some are penetrating primaries and some are produced from bremsstrahlung photons that transfer energy to electron secondaries within the Al shell. For ~MeV electrons and ~100–300 mil Al shields, the dose contribution due to these reconversion electrons is actually dominant over that from the penetrating primary electrons and secondary photons reaching the target. We found that using the adjoint technique to calculate electron spectra at the target (after passing though the shield) gave poor statistics for reconversion electrons; thus, for electrons at the 10 nm diameter target, we used a hybrid "double forward" calculation, whereby we used a forward Monte Carlo simulation to calculate electron spectra at the target and then a second forward simulation (per Figure 12) to obtain the dose response in the target. As noted in section 2.4, a single forward simulation of the whole system would take a prohibitively long time to build up statistics in a small target; thus, we took advantage of symmetry to aggregate spectra from the first simulation through the shield. For a target that is small compared with the inside radius of the shield, the spectrum reaching the target's surface is isotropic and equal in magnitude to the spectrum leaving the inside surface of the shield normal to that surface (that is, traveling along the shield's radius). Our simulations of electrons penetrating the shields showed that angular distributions were nearly isotropic up to about 30° off that surface normal, so we averaged over this range to improve statistics for the spectrum that reaches the target and then convolved that with the dose response in Figure 12.

Figure 13 shows just the photon response for select thickness of spherical Al shells with a 10 cm inner radius on a 300 nm diameter Si target. Likewise, Figure 14 shows just the electron response on a 10 nm target. We settled on 10 cm as representative of typical spaceflight geometry (typical box size) since, as shown in previous sections, the inner radius of the shield has little impact on the dose response.

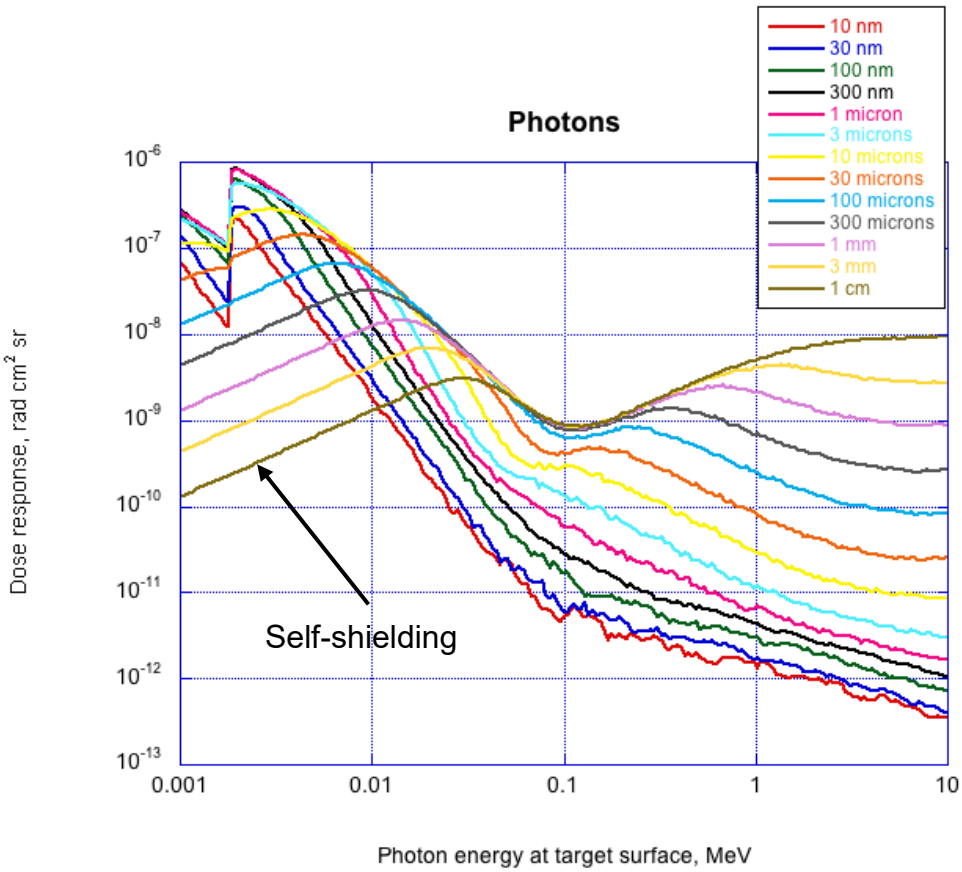

Figure 11. Forward Monte Carlo simulation of dose response for photons incident on bare silicon spheres of various diameters. A 300 nm target represents a reasonable, conservative case, capturing the response to low-energy photons, which should be more numerous than higher-energy photons inside spherical Al shields for realistic external electron environments. Thicker targets suffer from self-shielding and thinner targets are too thin to absorb the photons.

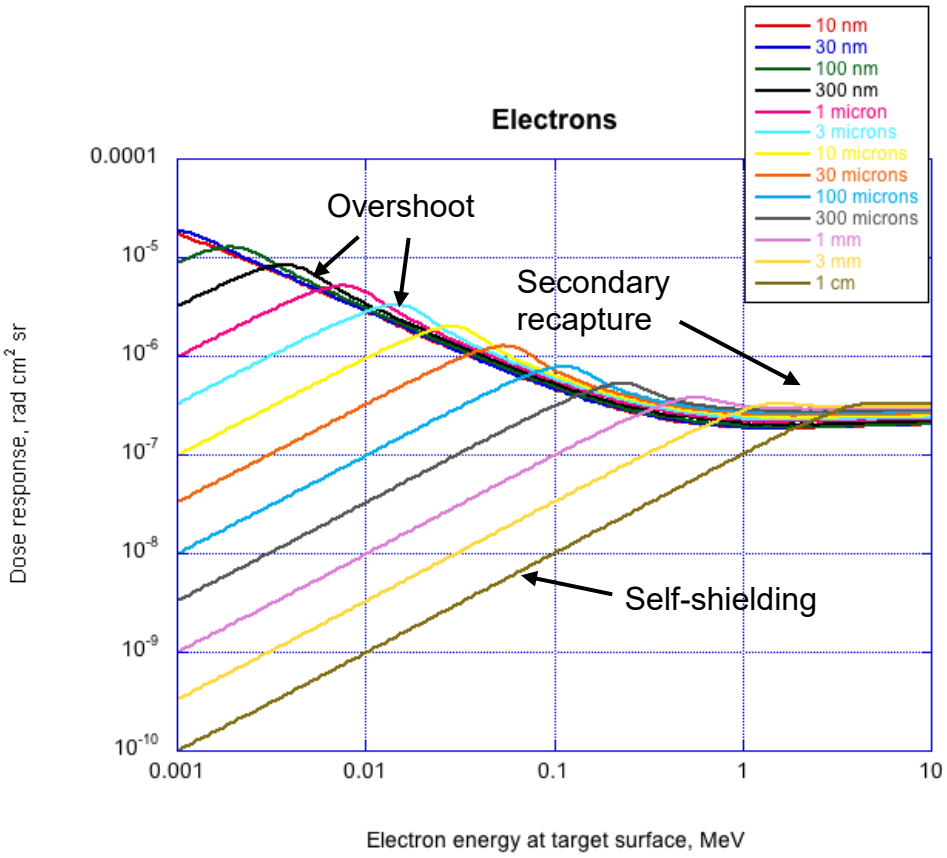

Figure 12. Forward Monte Carlo simulation of dose response for electrons incident on bare silicon spheres of various diameters. Undesired artifacts are indicated for diameters larger than 10 nm. The optimal choice for electrons that reach the target within the energy range shown, therefore, is a 10 nm target. Thicker targets mainly suffer from self-shielding.

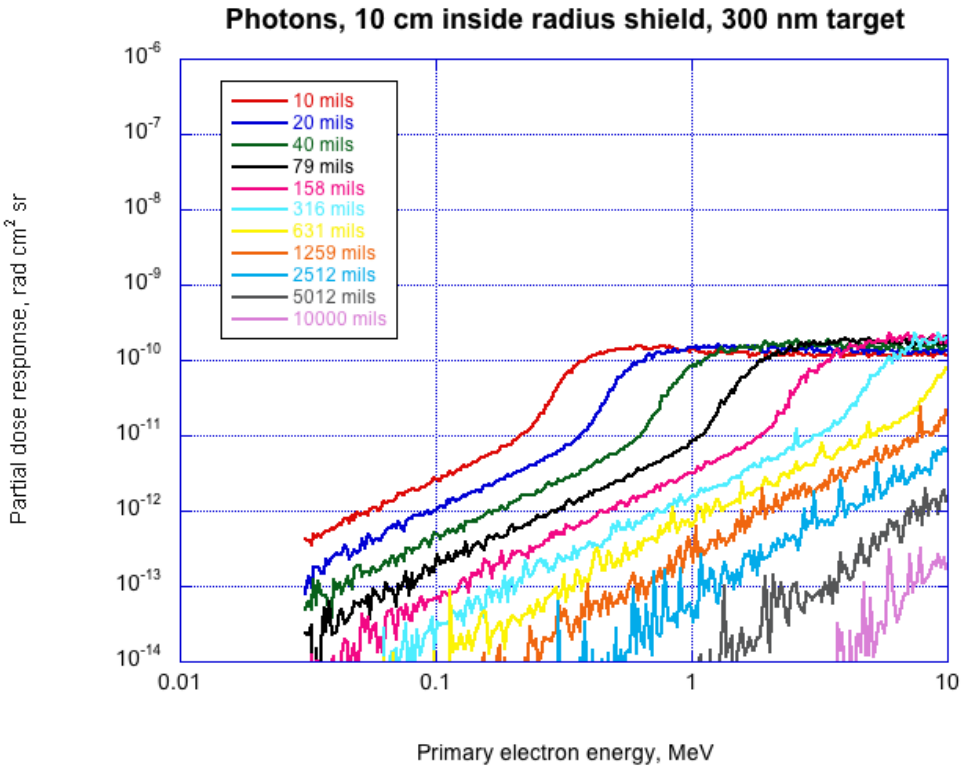

Figure 13. Dose response due to photons (x-rays) reaching a 300 nm diameter silicon target, as a function of primary electron energy and for a range of hollow-shell thicknesses. All shells have 10 cm inner radius. Dose response was computed with the combined adjoint and forward method described in the main text.

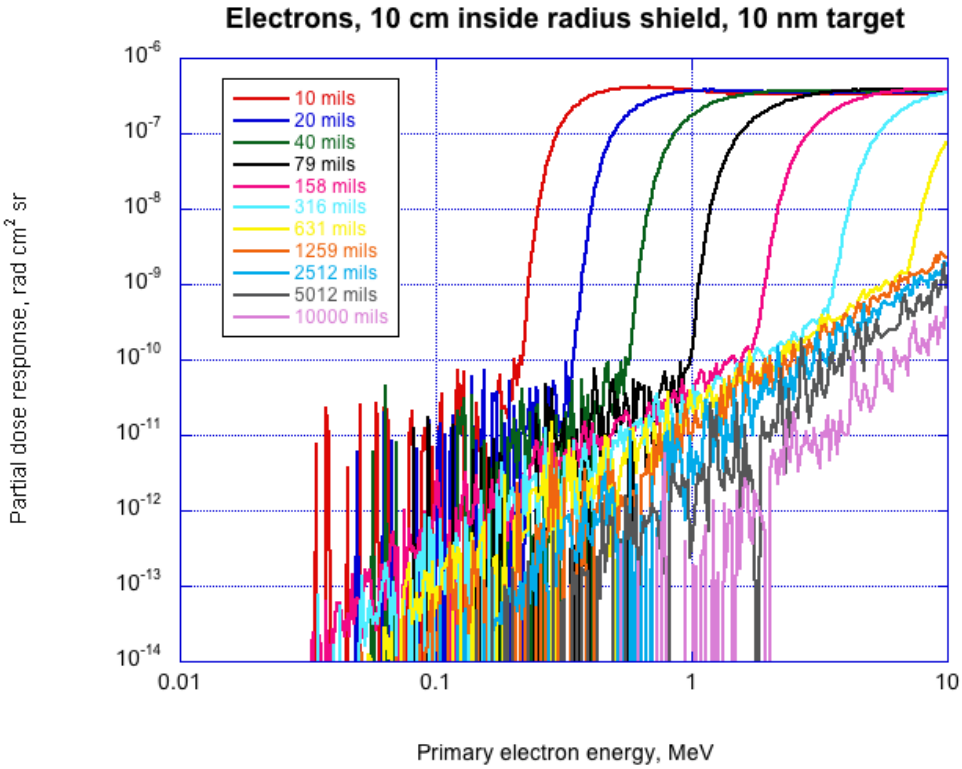

Figure 14. Dose response due to electrons reaching a 10 nm diameter silicon target, as a function of primary electron energy and for a range of hollow-shell thicknesses. All shells have 10 cm inner radius. Dose response was computed with the two-stage forward method described in the main text.

3. Construction of the Kernel

The kernel is the sum of the photon response in the 300 nm diameter Si target and the electron response in the 10 nm diameter Si target. In both cases, the sub-threshold response (below 75% of the range of an electron through the Al shielding, as given by [2]) needed to be fit with a power-law to reduce statistical scatter. Figure 15 shows the sum of the original computed (top) and fitted (bottom) responses. (As an example of the power-law fitting, the sub-threshold electron response is entirely responsible for the large spikes seen in the blue 10 mils curve in the top panel. A power-law is fitted to the integral of the electron-only response and then differentiated to obtain the parameters used in building the kernel. This procedure suppresses most of the statistical noise from the Monte Carlo calculation.) The kernel is built with the power-law fits replacing the computed values below 75% of the range, resulting in the smooth responses in the bottom of Figure 15.

Finally, the dose response obtained from the Geant4 calculations is in rad cm^2 sr, and must be divided by 4 π sr so that it becomes an average over all incident directions for consistency with the definition of the kernel file. The dose response is then $G(E_k; T_i)$ in Eq. (4), and can be stored directly in the kernel file. The kernel energy grid spans from ~30 keV to 10 MeV, and the depth grid spans from 10 mils to 10 inches Al.

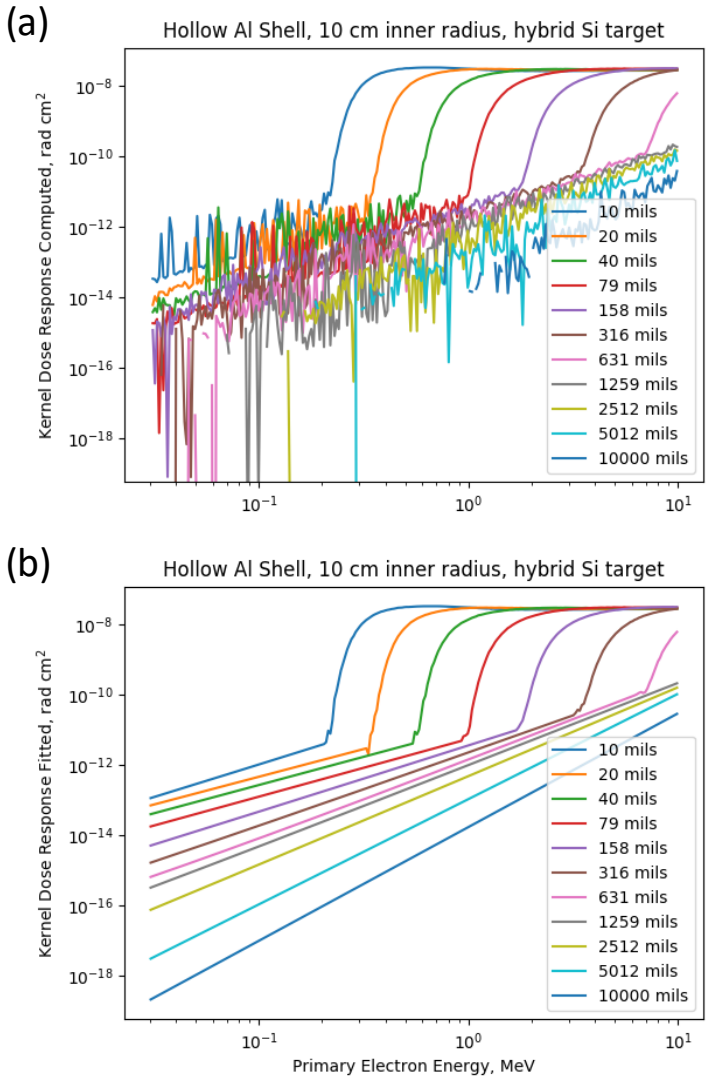

Figure 15. Summed electron and photon dose responses: (a) computed and (b) with sub-threshold response fitted to power-laws. The electron response is tabulated in a 10 nm diameter Si target and the photon response in a 300 nm Si target.

4. Validation

We can validate the new kernel by comparing it to two other related calculations. We can directly compare our hollow-shell geometry to a hollow-shell calculation with NOVICE (empc.com/novice-software). NOVICE results were provided by H. O'Donnell.

We use the fluence spectrum shown in Figure 16, which was generated for a synchronous orbit. It falls off steeply after 4–5 MeV and is zero beyond 7 MeV. Figure 17 shows four dose depth curves. Two curves are for solid-sphere geometry, provided by SHIELDOSE-2 and NOVICE. Up to about 300 mils, the solid-sphere calculations agree quite well. At thicker depths, SHIELDOSE-2 gives somewhat more dose than NOVICE.

For hollow-shell geometry, Figure 17 shows that the Geant4 kernel and NOVICE are in very close agreement. Both NOVICE and Geant4 show that less dose reaches the Si target for a hollow-shell geometry than for the same thickness of a solid-sphere shield up to about 200 mils Al, when bremsstrahlung begins to dominate the dose.

Because the three codes make different assumptions about the details of the physics and geometry, it is no surprise that there are some differences in their results. In the future, we hope to apply our approach to develop a solid-sphere kernel from Geant4 and possibly determine why NOVICE and SHIELDOSE-2 disagree at thicker depths.

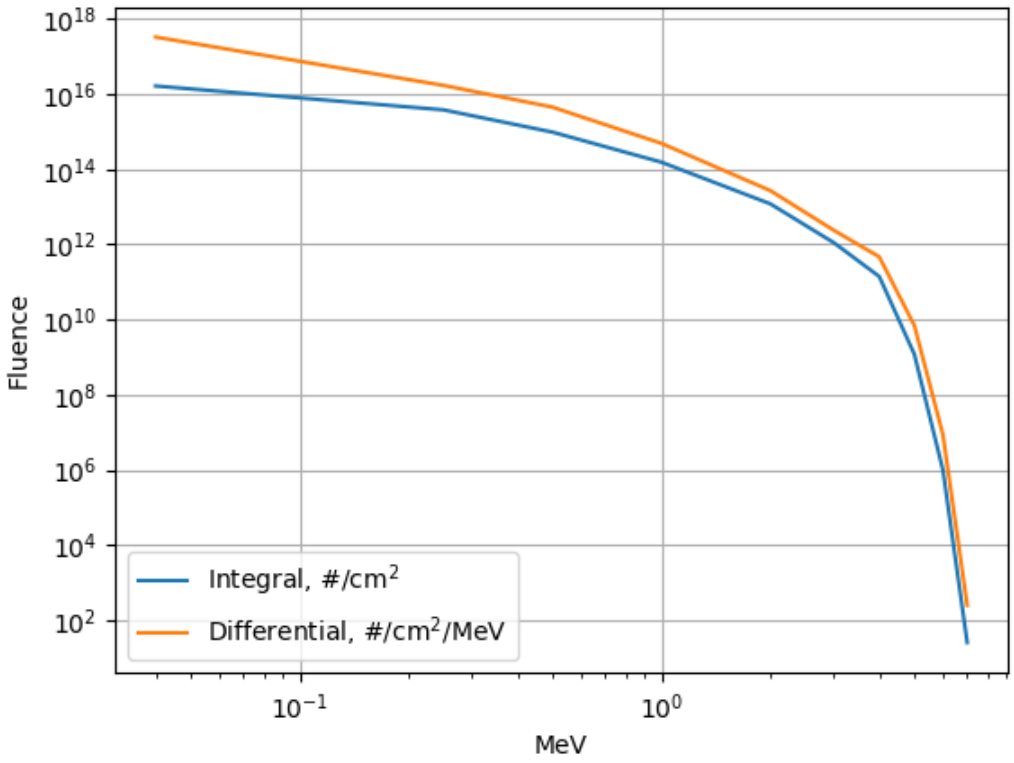

Figure 16. Test fluence spectrum, generated for a geosynchronous orbit.

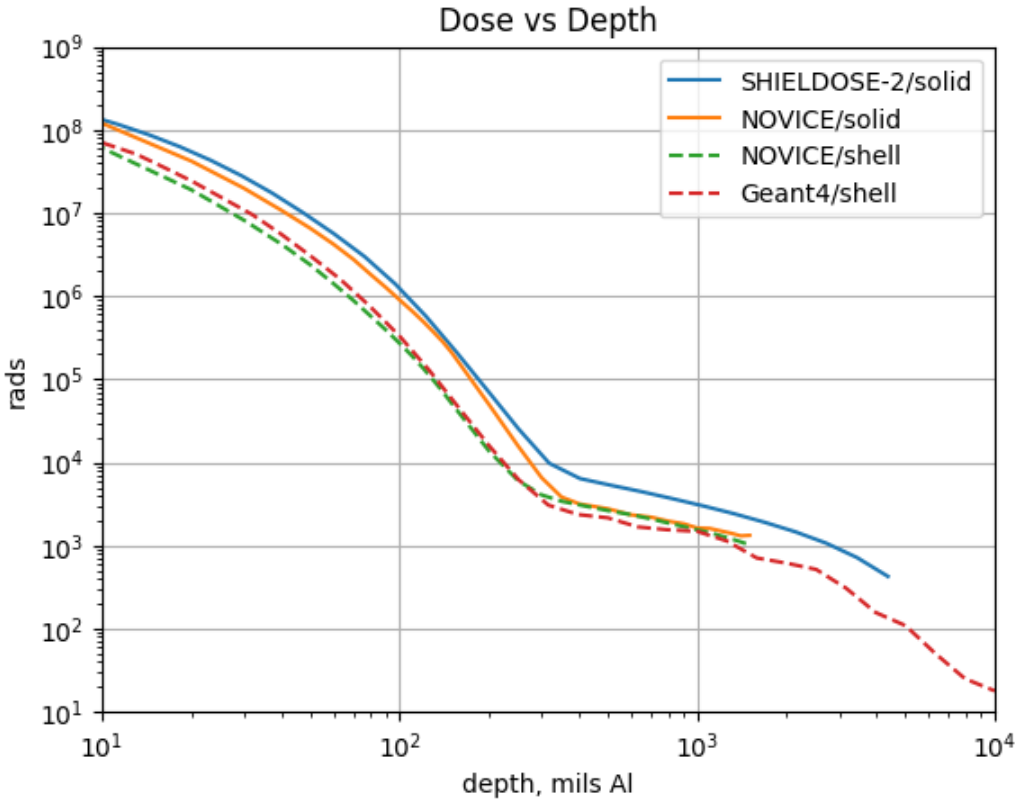

Figure 17. Dose vs. depth for solid-sphere and hollow-shell geometries for the spectrum in Figure 16. The curve labeled “Geant4/shell” was generated with the new kernel.

5. Summary

We have developed an AE9/AP9 kernel that can transform incident electron flux into dose versus depth for a silicon target inside hollow spherical aluminum shells. The kernel is captured in an XML text file that conforms to the AE9/AP9 kernel file format standard.

The fact that protons experience relatively little scattering compared to electrons at the energies of interest allows us to reuse the kernel already developed using the SHIELDOSE-2 dose-depth relation for solid spherical shielding, instead of developing a new one altogether, to give the dose-depth values for protons under a hollow spherical shell. For electrons, we have used the forward and adjoint Monte Carlo techniques as implemented in Geant4 to calculate dose-depth relations for silicon targets under a hollow spherical shell. We have combined simulations with different Si target sizes to account for different interaction behaviors with a finite target. We have also determined that, as long as the inner radius of the hollow spherical shell is larger than about 1 cm, varying that radius does not change the results, so we do not have to provide different dose-depth relations for different representative inner radii.

Along the way, we found that reconversion electrons, produced in the shield by bremsstrahlung photons that were previously generated there, can be the dominant cause of dose behind ~100s of mils of Al for ~MeV incident electrons. Since this effect requires a two-step conversion process (primary electron producing secondary photon producing tertiary electron), it is worth investigating further in the future in order to develop guidelines to ensure that shortcuts and approximations common to dose calculations do not inadvertently neglect an important physical process. This is especially important as adjoint methods become more widely used, as such methods must take care to properly represent secondary particle production processes.

We have shown that the hollow-shell kernel provides results similar to those from industry standard tools NOVICE and SHIELDOSE-2. The electron hollow-shell kernel can be released with a future version of the AE9/AP9 application to approximate dose inside spacecraft boxes, adding to the other geometries supported by kernels and by the SHIELDOSE-2 application. It will be helpful to compare hollow-shell and solid-shell geometries. When the two differ for a given mission, it indicates that a more detailed shielding analysis may be fruitful for assessing the radiation design.

6. References

[1] Allison, J. et al., Recent developments in Geant4, *Nucl. Inst. Meth. A 835*, 186–225, DOI:10.1016.j.nima.2016.06.125, 2016.

[2] Katz, L., and A. S. Penfold, Range-energy relations for electrons and the determination of beta-ray end-point energies by absorption, *Rev. Modern Phys. 24*(1), 28–44, 1952.

[3] Looper, M. D. et al., The radiation environment near the lunar surface: CRaTER observations and Geant4 simulations, *Space Weather 11* (4), 142-152, DOI:10.1002/swe.20034, 2013.

[4] Looper, M. D., *Adjoint Monte Carlo simulations and improved sector shielding calculations with Geant4*, Aerospace Report No. ATR-2018-00052, The Aerospace Corporation, El Segundo, CA, 2018.

[5] O'Brien, T. P., and B. P. Kwan, *Using pre-computed kernels to accelerate effects calculations for AE9/AP9: A displacement damage example*, Aerospace Report No. TOR-2013-00529, The Aerospace Corporation, El Segundo, CA, 2013.

[6] O'Brien, T. P. and P. Whelan, *Specification for radiation effects kernels for use with AE9/AP9*, Aerospace Report No. ATR-2015-02436, The Aerospace Corporation, El Segundo, CA, 2015.

[7] Seltzer, S. M., *Updated Calculations for Routine Space-Shielding Radiation Dose Estimates: SHIELDOSE-2*, Technical Report PB95-171039, National Institute of Standards and Technology, Gaithersburg, MD, December 1994.

AEROSPACE REPORT NO.
TOR-2018-02829

An AE9/AP9 Kernel for Ionizing Dose from Electrons Incident on Hollow Aluminum Shells

Approved Electronically by:

Joseph E. Mazur, PRINC DIRECTOR
SPACE SCIENCE APPLICATIONS LABORATORY
PHYSICAL SCIENCES LABORATORIES

Cognizant Program Manager Approval:

Thomas H. Hopp, PRINC DIRECTOR
ADVANCED SYSTEMS
SPECIAL PROGRAMS DIVISION
SPACE SYSTEMS GROUP

Aerospace Corporate Officer Approval:

Malina M. Hills, SR VP SPACE SYS
SPACE SYSTEMS GROUP

Content Concurrence Provided Electronically by:

T Paul O'Brien, SCIENTIST SR
MAGNETOSPHERIC & HELIOSPHERIC SCIENCES
SPACE SCIENCES DEPARTMENT

SY0467

AEROSPACE REPORT NO.
TOR-2018-02829

An AE9/AP9 Kernel for Ionizing Dose from Electrons Incident on Hollow Aluminum Shells

Technical Peer Review Performed by:

Brent A. Morgan, PROJECT LEADER SR
ADVANCED PROGRAMS
ADVANCED SYSTEMS
SPACE SYSTEMS GROUP

SY0467